Origin and characteristics of ancient organic matter from a high-elevation Lateglacial Alpine Nunatak (NW Italy)

Emanuele Pintaldi[1], Veronica Santoro[1,*], Michele Eugenio D'Amico[2], Nicola Colombo [1,3,4], Luisella Celi [1], Michele Freppaz M.[1,3]

[1]Università degli Studi di Torino - DISAFA, Largo Paolo Braccini 2, 10095, Grugliasco (TO), Italy

[2]Università degli Studi di Milano - DISAA, Via Celoria 2, 20133 Milano (MI), Italy

[3]Università degli Studi di Torino, NATRISK, Research Centre on Natural Risks in Mountain and Hilly Environments, Largo Paolo Braccini 2, 10095, Grugliasco (TO), Italy

[4]National Research Council, Water Research Institute, Strada Provinciale 35d, 00010 Montelibretti (RM), Italy

*_Correspondence to_: veronica.santoro@unito.it

Highlights

- The origin and composition of ancient organic matter from a high-elevation Alpine Nunatak were uncovered.
- More than 90% of organic carbon was stored in the stable mineral organic matter (MOM) pool.
- Based on NMR and FT-IR spectra the MOM fraction consisted of paraffinic substances (37-50%), cellulose and hemicellulose (29-37%).
- The organic matter originated from ancient alpine tundra that developed on the Nunatak since the end of Last Glacial Maximum.

Abstract

In high-mountain areas, Pleistocene glaciations and erosion-related processes erased most of the pre-existing landforms and soils. However, on scattered stable surfaces, ancient soils can be locally preserved for long periods, retaining valuable paleoenvironmental information. Such relict surfaces survived during glaciations either through coverage by non-erosive, cold-based, ice or as nunataks.

Thus, soils preserved on such surfaces retain excellent pedo-signature of different specific past climatic/environmental conditions. In this study, we performed a detailed chemical characterization of the organic material found in paleosols, discovered inside periglacial features on a high-elevation Lateglacial Alpine Nunatak (Stolenberg Plateau), above 3000 m a.s.l. (NW Italian Alps). The soil organic matter (OM) was separated in different pools by means of density fractionation, in order to separate the more fresh/unaltered free and occluded organic material (Light Fraction-LF) from the stable fraction chemically bound to mineral phase (Mineral Organic Matter - MOM). To better characterize the MOM fraction, this was further subjected to chemical fractionation, in order to separate the alkali-extractable OM (ext-MOM) from the fraction intimately bound to minerals. The obtained fractions were then characterized by chemical and ^{13}C nuclear magnetic resonance (NMR), and Fourier Transform Infrared (FT-IR) spectroscopy. The results indicated that the largest part (>90%) of organic carbon (OC) was stored in the stable MOM pool, characterized by a high degree of decomposition and consisting mainly of paraffinic substances, such as lipids and waxes (37-50%), cellulose and hemicellulose (29-37%). The OM likely originated from autochthonous, well-adapted, ancient alpine vegetation (alpine tundra) that grew on the Plateau during warm climatic phases since the end of the Last Glacial Maximum (LGM). These results further strengthen the paleoenvironmental reconstruction at the Stolenberg Plateau, which represents a Lateglacial Alpine Nunatak, and has acted as a biological refugia (at least) since the end of the LGM.

Keywords: soil organic matter, density/chemical fractionation, nuclear magnetic resonance, infrared spectroscopy, blockstream/blockfield, paleoenvironment

Introduction

The preservation of relict surfaces during glaciations occurred either through coverage by non-erosive, cold-based glacier ice, or as nunataks (Goodfellow, 2007). Relict, non-glacial surfaces are

distinguishable from glacial surfaces by the presence of large-scale morphologies, such as rounded summits, fluvial valleys, cryoplanation terraces and pediments, tors, blockfields, and/or saprolites (Goodfellow, 2007). In particular, blockfields, which are usually associated with mountain summits and plateaus (e.g., Ballantyne, 1998), have been used as indicators of non-erosive ice covers such as cold-based glaciers (e.g., Hättestrand and Stroeven, 2002) or nunataks (e.g., Ballantyne, 1998). The term nunataks, derived from Inuit language, indicates a mountain rising above inland ice (Dahl, 1987). More specifically, nunataks are isolated hills or mountain peaks that project above ice sheets and alpine-type icecaps (Fairbridge, 1968), which could act as refugia for isolated vegetation colonies. Thus, plants could survive the severe conditions of glacial periods on nunataks, with the latter serving as source for the rapid reoccupation of the later deglaciated landscape (Fairbridge, 1968). Although several studies have been focused on nunataks at high latitudes (e.g., Birks, 1994; McCarrol et al., 1996; Ballantyne et al., 1998; Paus et al., 2006), very few works studied nunataks in the European Alps (Schönswetter et al., 2005; Birks and Willis, 2008; Carcaillet and Blarquez, 2017; Pintaldi et al., 2021a; Pintaldi et al., 2021b), probably due to the intrinsic difficulties in finding relict surfaces preserved from glaciations.

Paleosols can be preserved under blockfields and blockstreams on nunataks (Pintaldi et al., 2021a; Pintaldi et al., 2021b). Ancient organic matter (OM) accumulated in paleosols generally consists of a complex mixture of several compounds, such as biochemical residues of polysaccharides, proteins, lignin, lipids, humic products and charcoal, which are mainly derived from vegetation as result of biotic and abiotic degradation (Nelson and Baldock, 2005; Kelleher and Simpson, 2006). Quaternary and Holocene paleosols represent a potentially important organic carbon (OC) reservoir, providing a unique opportunity for studying the mechanisms by which terrestrial C has been stabilized over millennial timescales (Zhou et al., 2014). Therefore, identifying and quantifying OM components are the prerequisites for understanding their origin and stabilization mechanisms (Xu et al., 2009; Zhou et al., 2014). Although some studies examined C compounds in paleosols with a focus on millennial-scale mechanisms of C stabilization (Monson et al., 2011; Marin-Spiotta et al., 2012; Zhou et al.,

2014), there is a paucity of works that investigated the chemical OM characteristics in high-elevated alpine paleosols (e.g., Favilli et al., 2008; Favilli et al., 2009).

Some authors have argued that, during the last glaciation, high-elevation plants might have survived on ice-free mountain tops within the strongly glaciated central parts of the Alps (Stehlik, 2002; Schönswetter et al., 2005; Kosiński et al., 2019). In the Monte Rosa massif (NW Italian Alps), in 2017, we detected well-developed Umbrisols, hidden inside periglacial features (blockstreams and blockfields), on a high-elevation plateau (Stolenberg Plateau, 3030 m a.s.l.) (Pintaldi et al., 2021a). Despite the thick and complete stony cover, and the extremely sparse vegetation, these soils showed OC stocks comparable to alpine tundra or even to subalpine forest soils and were classified by using ^{14}C dating as paleosols that have recorded the main warming climatic phases occurring since the end of the Last Glacial Maximum (Pintaldi et al., 2021b). This suggests that the environmental conditions on the Plateau were probably suitable for alpine plant life and pedogenesis, already 22-21 ka BP. Therefore, the Plateau was considered direct evidence of Lateglacial Alpine Nunatak, which acted as a possible biological refugium during glacial periods.

In this work, we aimed at: (i) unraveling the composition, origin, degree of decomposition, and related stabilization processes of the OM retrieved from the high-elevation paleosols found at the Stolenberg Plateau; (ii) relating the OM composition and stabilization processes to possible different climatic conditions, degradation regimes, and/or vegetation (type) modifications that these paleosols have experienced through time. To reach our aims, we performed OM physical and chemical fractionation, and characterization by solid state ^{13}C nuclear magnetic resonance (^{13}C NMR) and Fourier Transform Infrared (FT-IR) spectroscopies. To our knowledge, this study represents the first detailed chemical characterization of the soil OM from a high-elevated Alpine nunatak.

2. Materials and Methods

2.1 Study Area

The Stolenberg Plateau (3030 m a.s.l.) is located along the border between Valle d'Aosta and Piemonte regions, NW Italian Alps (LTER site Istituto Mosso), at the foot of the southern slope of Monte Rosa (4634 m a.s.l.) (Fig. 1). The area is a Site of Community Importance and a Special Protection Area (SCI/SPA IT1204220 "Ambienti glaciali del gruppo del Monte Rosa") (European Commission, 1992) belonging to the Natura 2000 network. The Plateau has a South-East orientation with a surface of ca. 13,500 m^2 and a mean slope below 13°. The Plateau has a mean annual air temperature of –2.4 °C (1988-2019) and a mean summer (June, July, August) air temperature of +4.4 °C; July is the warmest month, with a mean air temperature of +5.2 °C. The mean annual liquid precipitation is ca. 360 mm (1997-2019) while the mean cumulative annual snowfall is ca. 800 cm, with a snow cover lasting for at least 8 months (2008-2019).

The Plateau is covered by a thick stony layer, well organized in periglacial features (i.e., blockfields, blockstreams/sorted stripes, gelifluction lobes, tilted stones) (Pintaldi et al., 2021a). The parent material is composed of gneiss and mica-schists (Monte Rosa nappe, Pennidic basement), and metabasites (Zermatt-Saas unit) (Tognetto et al., 2021). The vegetation cover, almost absent (max 5%) or confined to small patches, is composed mainly of alpine species (e.g., *Silene acaulis, Carex curvula, Salix herbacea, Festuca halleri, Poa alpina, Ranunculus glacialis, Leucanthemopsis alpina, Cerastium uniflorum, Oxyria digyna*). As reported by Pintaldi et al. (2021a; 2021b), no relevant permafrost bodies are present at the site and no significantly negative soil temperatures occur under the blockstreams/blockfields. However, during the snow-free season, soil temperatures are generally colder under the periglacial features than in the surrounding snowbed soils covered by vegetation.

2.2 Soil survey, sampling and characteristics

In 2017, to protect the natural environment (European Commission, 1992) from the operational activities for the construction of a new cableway station, the largest part of the plateau was delimited. In the construction area three trenches were opened (2 to 10 m long, to a depth of around 1.2 m),

127 revealing well-developed soils within the blockfield/blockstreams, below the stony cover (soil
128 profiles P1, P2, and P3 in Fig. 1). These soils were characterized by dark, continuous and thick organic
129 C-rich A horizons (Fig. 1), and were classified as Skeletic Umbrisol (Arenic, Turbic), according to
130 IUSS Working Group WRB (2015). At first, 27 soil samples were collected from all genetic horizons
131 in the profiles at different depth (~ 10-70 cm), from which 7 samples were selected (details in Pintaldi
132 et al., 2021a). Specifically, these samples were collected from A horizons in the profiles (between 10
133 and 60 cm depth), according to the sampling schemes reported in Fig. 1 (A, B, C): two from profile
134 P1 (1, 2); three from profile P2 (7, 8, 9); two from profile P3 (3, 5). Moreover, one soil sample was
135 collected in the only fully vegetated patch of the plateau (P4), at 10-20 cm depth (A horizon). The
136 selection of samples was based on the available ^{14}C radiocarbon dates (Pintaldi et al., 2021b), which
137 spanned from 4.4 to over 22 ka BP, and corresponded exclusively to the main interstadials and warm
138 phases that have occurred since the end of the Last Glacial Maximum (LGM).
139 The soil texture was generally loamy sand or sandy loam, pH extremely to moderately acidic, and
140 carbonates were absent (Tab. 1). The weathering degree of the material was advanced, particularly
141 below the stony cover and in the discontinuous Bw horizons (Pintaldi et al., 2021a). The oxalate
142 extractable Fe and Al (Fe_o and Al_o, Schwertmann 1964) were below 3 g kg^{-1}, while dithionite
143 extractable Fe (Fe_d, Mehra and Jackson, 1960) was between 14 and 23 g kg^{-1}; the Fe_o/Fe_d ratios were
144 low, demonstrating an advanced aging state of the soil material (Stützer, 1999; D'Amico et al., 2019)
145 (Tab. 1). The high pH measured in a 1M NaF suspension verified the presence of abundant short
146 range-order minerals (allophane and imogolite-type materials) in many horizons, not related to age
147 (data not shown).
148 The Total Organic Carbon (TOC) content reached maximum values of ca. 20 g kg^{-1} in the A
149 horizons of profiles P1 and P2, and over 10 g kg^{-1} in profile P3; despite the extremely sparse
150 vegetation cover, the soil C stocks were up to ~ 5 kg m^{-2}.
151 Geophysical investigations indicated that these hidden soils are widespread on the Plateau. The
152 detailed description of the soil profiles, as well as their physical and chemical properties, distribution,

and thickness are reported in Pintaldi et al. (2021a), while their age, origin, and possible paleoenvironmental reconstruction are reported in Pintaldi et al. (2021b).

2.3 Organic matter fractionation and characterization

A physical fractionation of OM based on density (Cerli et al., 2012) was preliminarily applied to separate free and occluded organic material from the fraction chemically bound to mineral phase, with the specific aim of isolating the most stable fraction, avoiding the influence of fresh and unaltered organic materials. In particular, we performed the density fractionation on the selected eight soil samples collected from A horizons on the Plateau. The soil samples were air-dried and sieved to 2 mm. Density fractionation was performed using sodium polytungstate at a density of 1.6 g cm^{-3} and applying the appropriate sonication energy selected after preliminary tests. We obtained three different fractions: free particulate organic matter (fPOM), particulate organic matter occluded into soil aggregates (oPOM), and mineral-associated organic matter (MOM). However, based on preliminary tests, as the quantities of the separated fPOM and oPOM fractions were too low, they were merged into one and called Light Fraction (LF) thereafter. We separated, washed, dried, and analyzed the fractions for their mass, and C and N content by dry combustion with an elemental analyzer (Elementar Unicube, Langenselbold, Germany).

To better characterize the MOM fraction, this was further treated with NaOH to separate the alkali-extractable OM from the fraction intimately bound to minerals (Schnitzer, 1982). We treated the samples with a 0.5 N NaOH solution (soil:liquid ratio 1:10) under N_2 flux, acidified the alkaline extractable MOM (ext-MOM) using HCl, and subsequently freeze-dried it. The ext-MOM was then analyzed for the C and N content. We corrected the data for ash and moisture content.

Based on the age of the original bulk soil samples, from which we obtained the different OM fractions, we selected six LF and the corresponding ext-MOM samples for the chemical characterization through high-resolution solid-state ^{13}C CPMAS nuclear magnetic resonance (^{13}C

CPMAS NMR) spectroscopy. We recorded solid state ^{13}C NMR spectra on a Jeol ECZR 600 instrument, operating at a frequency of 150.91 MHz, at room temperature with the sample at magic angle, rotating at 20 kHz. Samples were packed in cylindrical zirconia rotors (3.2 mm o.d.), with a sample volume of 60 µl. All experiments employed the RAMP-CPMAS pulse sequence (1 H 90° pulse = 2.0 µs; contact time = 1 ms; optimized relaxation delays of 2 s; 5000 scans for LF samples, 35000 scans for ext-MOM samples) with the TPPM 1 H decoupling (rf field = 112 kHz) during the acquisition period. We referenced the ^{13}C chemical shift scale with the resonance of glycine as an external standard. We divided the ^{13}C NMR spectra into the following regions: 0–45 ppm; 46–60 ppm; 61–110 ppm; 111–155 ppm; 156–165 ppm; 166–190 ppm, and elaborated the spectra using the Delta v5.3.1 software (Jeol Ltd., Japan).

Fourier Transform Infrared (FTIR) spectra of LF and ext-MOM were obtained in the 4000-400 cm^{-1} range using a Perkin Elmer Spectrum 100 (USA) instrument, in the attenuated total reflectance (ATR) mode, with a diamond crystal, using 32 scans per spectrum and a resolution of 4 cm^{-1}. We identified the following bands: 3400 cm^{-1} (hydrogen bonded –OH and amine N-H bonds); 2923 cm^{-1} and 2852 cm^{-1} (–CH_2– and CH stretching of aliphatic compounds, respectively); 1720 and 1630 cm^{-1} (–C=O asymmetric and symmetric stretching of carboxyl acids, esters, ketones and I amides); 1630-1600 cm^{-1} (C=C of aromatic groups); 1552 cm^{-1} (–CONH– of II amide); 1512 cm^{-1} (skeletal aromatic stretching of lignin); peaks 1460 and 1380 cm^{-1} (–CH_2– and –CH_3 bending); 1150–1050 cm^{-1} (alcoholic and polysaccharidic C–O and OH stretching and bending) (Piccolo and Stevenson, 1982; Oddi et al., 2019; Agnelli et al., 2021).

3. Results

3.1 Organic carbon distribution

The TOC content of bulk soil samples spanned from around 10 g kg^{-1} in the oldest samples (P3-3 dating back to the end of LGM), to over 20 g kg^{-1} in sample P1-1, dated from the Holocene Climatic

Optimum - HCO (Tab. 2). Only a small part of TOC was represented by the LF fraction (around 3.1-7.4% of bulk soil TOC), except in sample P1-1 (12-8%), in the near-surface sample P2-9 (14.3%) and in the vegetated P4 (9.1%). The remaining fraction was represented by MOM (Tab. 2), which stored between 86 and 97% of TOC, with the highest value in the oldest sample P3-3. The C contents in the LF ranged between 123 and 312 g kg^{-1}; we measured the highest value in the vegetated P4. Otherwise, no differences were associated to either age or depth of sampling. In the MOM, C contents were between 7 and 15 g kg^{-1}. Also in this case, we did not observe specific trends with either age or depth; however, we measured the highest values in samples with ages between 6.4 and 8.6 cal. ka BP, i.e. from the HCO. The TN distribution (Tab. 2) was similar, with LF accounting between 1.3 and 8.5% of TN and MOM, ranging between 91 and 99%, with the highest value in sample P3-3, dated from the end of the LGM. The N content of the LF spanned between 5 and 14 g kg^{-1}, with the highest values in surface sample P2-9 and vegetated P4. In the MOM, N content was overall around 1 g kg^{-1}. We found the highest C/N ratio values in LF samples, particularly in subsurface samples P1-1, P2-7, and P2-8, while in MOM the C/N ratio was rather low, with lowest values in surface sample P2-9 and vegetated P4. The C content in the ext-MOM ranged between 451.7 g kg^{-1} (P2-8) and 601.0 g kg^{-1} (P2-7), while the N content spanned from 44.8 (P1-1) to 79.1 g kg^{-1} (P4). Regarding the C distribution, the ext-MOM fraction was between ca. 24 (P2-9) and 47% (P1-1) of C of MOM, while N accounting between 25 (P2-9) and ca. 60% (P1-1 and P1-2). The highest C/N ratio values were in samples P1-1 and P2-7 (ca. 12), while the lowest ones were in the near-surface samples P1-2, P2-9 and P4 (8 and 7, respectively).

3.2. OM chemical characteristics

3.2.1 ^{13}C NMR

The solid-state high-resolution ^{13}C CPMAS NMR spectra and the relative C distribution of the LF samples showed specific patterns among samples (Fig. 2 and Tab. 3). In particular, all samples except

P4 and P2-9 presented a prominent signal in the 0–45 ppm alkyl region (long chain aliphatic moieties), accounting for 64 (P3-3, P3-5) and 75% (P1-1, P2-7) of total C, with relatively defined signals at 30 and 33 ppm attributable to paraffinic C of lipids and waxes (Oddi et al., 2019). Conversely, in P4 and P2-9 this region accounted only for 25 and 34 % of total C, respectively, and it was balanced by a larger contribution (52.5 and 44.8%) of the 61–110 ppm O-alkyl region, likely due to cellulose and hemicelluloses (Merino et al., 2018). In the other samples the O-alkyl C contributed to 15-21% of total C.

The samples also showed a signal in the 46–60 ppm region (C in branched aliphatics, amino acids, and OCH_3 groups). This signal was the lowest in P1-1 and P2-7 (3.5%), between 6.0 and 7.0% in samples P3-3 and P3-5, and around 8.0–9.0% in P2.9 and P4. In the 111–155 ppm (aromatic C) region, we observed a greater variability, as the signal represented 0.4 - 0.6% of total C in samples P1-1 and P2-7, 3.0–6.7% in P3-5 and P3-3, and the highest values (7.2–8.7%) in P2-9 and P4. The 156–165 ppm signals (C in phenolic groups) were generally low (<1%) and the 166–190 ppm region (C in carboxyl, amide, and ester groups) ranged between 3.7 (P2-7) and 5.7% (P3-3).

The solid-state ^{13}C NMR spectra and the relative C distribution of the ext-MOM fractions showed a dominance of alkyl C and O-alkyl C compounds (Fig. 2 and Tab. 4). More specifically, all samples presented a prominent and broader signal in the 0–45 ppm region with respect to LF spectra, from 37 (P3-3) to 50% (P2-9). We also observed in all ext-MOM spectra prominent signals in the 61–110 ppm, accounting from 29 (P2-9) to 37% (P3-3) of total C. We observed other relevant signals in the 46–60 ppm region, with intensity between 7.9 (P2-9) and 14% (P3-3). By contrast, the intensity of signals in the 111–155 ppm and 156–165 ppm regions remained very low, indicating a scarce presence of aromatic and phenolic compounds. In the 166–190 ppm region the intensity of C attributed to carboxyl groups increased, being 7.5 and 8.4% in P1-1 and P2-7, around 4-5% in P3-5 and P3-3, and 8-9% in samples P2-9 and P4.

3.2.2 FT-IR

The FT-IR spectra of the LF samples (Fig. 3a) all showed a sharp band in the 1100–1000 cm^{-1} range, due to C−O stretching of phenols and/or alcoholic OH groups, indicating the presence of saccharides. The band at 1630 cm^{-1} (C−O stretch of COO- groups and I amides) was evident in all samples except P3-3, while we observed bands at 2923 and 2850 cm^{-1} (aliphatic C−H stretching) in P2-7 and P3-5. P2-7, P2-9, and P3-5 displayed a shoulder at 1730 cm^{-1}, due to the C=O stretching of different functional groups (mainly carboxyls). A band at 1540 cm^{-1} was also evident in sample P2-9, ascribable to the presence of proteinaceous material (Piccolo and Stevenson, 1982). Samples P1-1, P2-7, P2-9, and P4 also displayed a peak at around 1470 cm^{-1} due to −CH2 bending, while a peak at 1380 cm^{-1} was present in samples P2-7, P2-9, and P3-5 (C–O stretching of phenolic C–OH, asymmetrical stretching of CO– groups, and amine groups in heterocyclic and aliphatic structures) even if not so intense.

The FT-IR spectra of ext-MOM samples showed a wider variability and presence of different bands (Fig. 3b). Samples P1-1, P2-7, P2-9, and P3-5 displayed a moderately intense peak at 1080 cm^{-1}, with a shoulder at 1123 cm^{-1}, due to C–O stretching of phenols and/or alcoholic OH groups. In sample P3-3, the 1080 cm^{-1} band was instead accompanied by a band at 1037 cm^{-1}, which in turn was present also in sample P2-7, even if much less pronounced and shifted to 1030 cm^{-1}. Sample P4 displayed a broad band at 1010 cm^{-1}, more similar to those observed in LF samples, and a weak band at 1624 cm^{-1} (C=C of aromatic groups and I amides) which, on the contrary, was much more pronounced in the rest of the samples and shifted to 1636 cm^{-1} in P2-9. Samples P1-1, P2-7, and P4, also displayed two very weak bands at 2923 and 2850 cm^{-1} (aliphatic C-H stretching, not shown), while samples P1-1, P2-7, P3-2, P3-5, and P4 showed a small band at around 1460 cm^{-1}, due to $–CH_2$ and $–CH_3$ asymmetric bending. In general, in the ext-MOM samples, the broad peak at around 3450-3350 cm^{-1} was more pronounced than in the LF samples, and was asymmetric, with a shoulder at around 2900 cm^{-1}, possibly due to aliphatic C-H stretching. The interpretation of the FT-IR spectra is based on data reported in Celi et al. (1997, 2010) and Agnelli et al. (2021), and references therein.

4. Discussion

4.1 C and N distribution and stabilization processes

Despite the lack of vegetation and the presence of periglacial features, all soil samples exhibited considerable TOC and TN contents, coupled with a rather low TOC/TN ratio. The preservation of OM in such paleosols may have been due to numerous factors that combine the severe constraints determined by low temperatures and acidic pH (Budge et al., 2011) with different stabilization mechanisms, such as OM redistribution at different depths due to cryoturbation processes (e.g., van Vliet-Lanoë et al., 1998; Hormes et al., 2004; Bockheim, 2007), chemical recalcitrance and interaction with the mineral phase (e.g., Mikutta et al., 2006; Kaiser et al., 2007).

Our results show that the greatest part of soil TOC was stored in the stable MOM fraction (86-97%), while the contribution of LF was less important but very variable, ranging from 3 to 14% of TOC. As expected, the highest LF values were observed in the reference sample P4, where a current vegetated snowbed patch is present. Here, the LF fraction was likely related to the input of plant residues through locally growing roots and litter. The material showed a high N content, probably caused by the presence of N-rich species typical of harsh high-elevation habitats (Mainetti et al., 2021), coupled with a great microbial N immobilization dominating N processes at low soil temperature (e.g., Freppaz et al., 2008). Low soil temperatures also participate in OM preservation, by slowing down early decomposition of fresh organic matter. Similar LF contents were found in the surface sample P2-9, where the input of recent OM derived from local plants is much smaller, partly counterbalanced by aeolian inputs of materials derived from nearby plant communities (Pintaldi et al., 2021b) and, more surprisingly, in the subsurface horizon P1-1. Notwithstanding the long residence time of TOC in P2-9, that dated ~17.7 ka, LF was likely fed by fresh input from sporadic vegetation and aeolian materials, but it showed a lower C/N ratio than the other horizons of the same profile. This was due to the decrease of C rather than to a relative increase of N, indicating that the organic material has

304 undergone a more intense degradation along the profile with respect to P4. The accumulation of LF
305 in the deep P1-1 is probably related to cryoturbation phenomena, which largely characterize the study
306 area (Pintaldi et al., 2021b) and caused OM redistribution along the profile (van Vliet-Lanoë et al.,
307 1998; Hormes et al., 2004; Bockheim, 2007).
308 Despite these differences, the greatest part of TOC was stored in the MOM fraction. This fraction
309 showed a low C/N ratio in all samples, hypothesizing a long residence time of the organic material
310 associated to minerals, since such low values are usually observed in milder climates and at lower
311 elevation (Tan et al., 2007; Conen et al., 2008; Baisden et al., 2002). This indicated that sorption
312 processes on minerals and interaction with metal ions in these ancient soils played a fundamental role
313 in OM preservation (Wiseman and Püttmann, 2006), prolonging its mean residence time (Saggar et
314 al., 1996). This is consistent with the relatively high pedogenic weathering degree of the soil materials
315 and the consequent prevalence of crystalline forms over poorly crystalline ones (Fe_d >>Fe_{ox}), with
316 much higher Fe_d values than those found in topsoils in nearby mountain areas (e.g., D'Amico et al.,
317 2020). Amorphous Fe and Al (hydr)oxides interact very efficiently with OM, while more crystalline
318 (hydr)oxides generally offer lower surface area and number of sorption sites (Mikutta et al., 2006;
319 Kaiser et al., 2007; Celi et al. 2020). However, with increasing soil weathering and acidification, more
320 crystalline Fe and Al (hydr)oxides may conserve a large specific surface area (Kleber et al., 2021),
321 still able to bind recalcitrant compounds efficiently (Kramer et al., 2012; Hall et al., 2016), thus
322 becoming more important in OM stabilization over time (e.g., Eusterhues et al., 2003; Mainka et al.,
323 2021). This may be further confirmed by the fact that almost 40-50% of MOM was extracted with
324 NaOH, which can hydrolyze OM-mineral bonding.
325 Thus, the sharp predominance of the MOM fraction and the chemical protection offered by the
326 presence of Fe and Al (hydr)oxides could explain the impressive ^{14}C age of these paleosols, thus
327 confirming an advanced pedogenesis and a long OM mean residence time. Interestingly, excluding
328 the samples P2-9 and P1-1, the C stored in the MOM fraction tended to increase with soil age,
329 spanning from 90% in the youngest soil sample P4, dated around 4.2 ka, to 97% in the oldest sample

P3-3, dated around 21-22 ka cal. BP. However, we did not observe a clear trend supporting such observation, probably because of the strong influence of cryoturbation processes, which, acting across millennia, strongly decomposed and mixed plant fragments within soil matrix, favoring the interaction with the mineral phase (i.e., Egli et al., 2009; Celi et al., 2010). Furthermore, in permafrost-affected soils (past or present), OM has been preserved due to the prevailing cold conditions that constrain or slow down its decomposition (Hobbie et al., 2000; Weintraub and Schimel, 2003; Celi et al., 2010). This preserved OM is however often in a fragmented, particulate form (POM) in present-day permafrost-affected arctic soils (e.g., Gubin and Lupachev, 2008; Lupachev et al., 2017), as the conditions created by both ice at shallow depths and waterlogging create a much harsher habitat for decomposer communities in high-latitude tundra soils.

4.2 SOM fraction characteristics

The LF showed important chemical features, with specific differences among samples. Parallel to a larger content, the LF P4 and P2-9 were characterized by a sharp dominance of cellulose and hemicellulose (45-52%) followed by a lower contribution of lipides and waxes (25-34%) with a consequent lower alkyl-C/O-alkyl-C ratios compared to the other samples. Although the respective original soil samples came from very different epochs (HCO and ELID, respectively), both fractions appeared to be mainly composed of fresh, almost unaltered present-day vegetation, in line with the overall modern age attributed to the plant fragments found in these paleosols (Pintaldi et al., 2021b). Conversely, the LF P1-1, even if present in quantities comparable to LF P4 and P2-9, showed a sharp dominance of alkyl C and a lower contribution of cellulose and hemicellulose residues, as deduced by both NMR and FT-IR spectra. LF P2-7 showed a chemical composition comparable to LF P1-1. Despite being probably modern, both pools are derived from bulk soil samples belonging to the warm HCO that occurred between 10,000 and 5,000 yr. BP (Mercalli, 2004; Orombelli, 2011). As the LF consists mainly of plant-derived debris (Golchin et al., 1994; Wagai et al., 2009), without interaction

355 with the mineral phase (Cerli et al., 2012), such unprotected fractions underwent a considerable
356 decomposition with the selective enrichment of lipids and waxes. These compounds were
357 characterized by a high chemical recalcitrance (Ziegler and Zech, 1989; Cerli et al., 2008; Agnelli et
358 al., 2021 and references therein reported), further enhancing the accumulation of the organic material
359 in the subsurface horizons where microbial degradation is strongly constrained by limited O_2
360 diffusion.

361 Similar to the previous ones, LF samples P3-3 and P3-5 showed a dominance (64%) of paraffinic
362 components, and this was particularly evident in sample P3-5, where the C in cellulose residues was
363 lower (15-21%). These samples derived from soil samples dated around 22 and 13 cal. ka BP,
364 respectively, and belonged to the LGM-ELID (Early Lateglacial Ice Decay) transition and the
365 Bølling-Allerød interstadial (Pintaldi et al., 2021b). The dominance of recalcitrant compounds found
366 in these samples was also reflected in the alkyl-C/O-alkyl-C ratio, thus confirming their relative
367 accumulation (Golchin et al, 1994; Budge et al., 2011). During microbial decomposition, organic
368 compounds derived from plants are increasingly replaced by those derived from microbes (Berg and
369 Meentemeyer, 2002). Moreover, in less extreme habitats (subalpine grasslands) the C paraffinic
370 compounds tend to increase in litter with increasing time of decomposition, especially in forb organic
371 materials (Oddi et al., 2019).

372 The ^{13}C NMR signals ascribable to aromatic C were the lowest in the deeper samples P1-1 and
373 P2-7, confirming a higher degree of decomposition. Although elevation may strongly affect both
374 vegetation composition and degradation rate (Budget et al., 2011), we can infer that LF samples could
375 be attributed to the autochthonous present-day alpine tundra species growing in or close to the study
376 area.

377 When extracting the NaOH-soluble fraction from the organic pool intimately associated with minerals
378 (ext-MOM), the obtained pool showed a less pronounced variability among samples, compared to LF
379 and a general predominance of paraffinic substances, such as lipids and waxes (37-50%), and
380 cellulose and hemicellulose (28-37%). As reported by Adhikari and Yang (2015), Fe oxides may

provide a selective stabilization of aliphatic substances, contributing considerably to their accumulation in soil (Sodano et al. 2016). The dominance of recalcitrant compounds, such as waxes/lipids, was also reported by Celi et al. (2010) in sporadic permafrost-affected soils, thus confirming that such substances dominate OM pools in cold environments (Hobbie et al., 2000). The presence of amino acids (8-14%) may further suggest the contribution of microbial communities (Freppaz et al., 2021) from soil biological crusts, especially in early stage of soil formation (Agnelli et al., 2021). Furthermore, the considerable presence of carboxyl groups (4-9%), also shown by the peak at 1630 cm^{-1} in the FT-IR spectra, may suggest that this material was subjected to relatively high oxidation processes favoring a strong interaction with the mineral phase. Overall, the composition of ext-MOM samples was comparable to those reported by Dymov et al. (2015), who indicated a dominance of alkyl-C compounds and a lower aromaticity in soils of alpine tundra. This finding was also consistent with other studies worldwide, which reported a lower aromaticity in arctic tundra and permafrost-affected soils (Dai et al., 2001; Lodygin et al., 2014), probably related to severe climatic condition, such as low temperature, high moisture content, anaerobic conditions and a shorter period of biological activity (White et al., 2004). Moreover, our results are comparable to those reported by Zhou et al. (2014), who found a dominance of alkyl-C and O-alkyl C compounds coupled with a lower presence of aromatic C in Holocene paleosols. High alpine tundra soils in the Tibetan plateau also showed lower aromaticity compared to lower elevation soils (Li et al., 2017). Based on the presence of carboxyl groups, we can infer that the degradation processes have been active across millennia, forming reactive groups that interacted with the mineral phase, thus offering a chemical protection against further decomposition. However, we did not observe a significant correlation between chemical markers, such as the alkyl-C/O-alkyl-C ratio or the content of carboxyl groups, and soil samples age. The cryoturbation processes occurring during millennia could have not only redistributed OM quantity at different depths (e.g., van Vliet-Lanoë et al., 1998; Hormes et al., 2004; Bockheim, 2007), but also modified the composition of the remaining material, thus masking the time-related processes.

Our results, coupled with ^{13}C values ascribable to alpine vegetation (Pintaldi et al., 2021b), confirmed that the Plateau, during warming phases, was probably colonized by well-adapted autotrophic organisms belonging to alpine tundra ecosystems, dominated by perennial grasses, forbs, shrubs, and biological soil crusts consisting of cyanobacteria, lichens, and mosses (Kauffman and Pyke, 2001; Agnelli et al., 2021). On the other hand, the content of aromatic compounds, generally associated with combustion processes (Shiau et al., 2017; Merino et al., 2018), was rather low, thus reinforcing and confirming our hypothesis on the biological origin of this ancient OM, although chemical features showed a mixed material that made not possible to distinguish a clear bio-climatic pattern. Therefore, despite the profound difference in age among samples, we assume that the Plateau might have been repeatedly colonized by similar alpine vegetation during warm climatic phases.

5. Conclusion

In this work, we investigated the chemical characteristics of ancient OM stored in the hidden paleosols of a high-elevation Lateglacial Alpine Nunatak. Our results suggest that the OM originated from autochthonous, well-adapted ancient alpine vegetation and other autotrophic organisms belonging to alpine tundra ecosystems, that grew on the Plateau at the time of soil formation (i.e., mostly during warming phases since the end of the LGM).

The greatest part of TOC was stored in the stable MOM, while the contribution of LF was less representative. The MOM fraction was characterized by a high degree of decomposition, according to the ancient age of paleosols. Apparently, the C stored in this fraction tended to increase with increasing age of soils samples, thus suggesting that, over time, the OM would be progressively stabilized and protected through the interaction with the mineral phase (especially within the crystalline Fe and Al (hydr)oxides). The NMR and FT-IR spectra revealed that the MOM fraction mainly consisted of paraffinic substances (lipids and waxes), cellulose, and hemicellulose. Despite the profound difference in age among soil samples, we suppose that the Plateau might have been

repeatedly colonized by similar alpine vegetation during warming phases, since we did not detect significant differences in chemical composition. The chemical signature of the OM, which clearly reflected the characteristics of past vegetation growing on the Plateau during warm climatic phases, was ascribable to the typical alpine vegetation present currently in the surrounding. Thus, the results further reinforce our paleoenvironmental reconstruction, supporting the fact that the Stolenberg Plateau represents a nunatak, which has acted as biological refugia (at least) since the end of the LGM.

Acknowledgments

This study was supported by European Regional Development Fund in Interreg Alpine Space project Links4Soils (ASP399): Caring for Soil- Where Our Roots Grow (http://www.alpinespace.eu/projects/links4s oils/en/the-project). Many thanks to Monterosa Ski Resort (Monterosa 2000 and Monterosa SpA project stakeholders) for providing logistical support.

Authors' contribution

Emanuele Pintaldi: conceptualization, investigation, data curation, writing – original draft.

Veronica Santoro: formal analysis, visualization, writing – original draft.

Michele E. D'Amico: investigation, validation, writing – review & editing.

Nicola Colombo: visualization, writing – review & editing.

Luisella Celi: resources, validation, writing – review & editing.

Michele Freppaz: project administration, funding acquisition, supervision.

Declaration of interests

The authors declare that they have no known competing financial interests or personal relationships that could have appeared to influence the work reported in this paper.

References

Adhikari, D., Yang, Y., 2015 Selective stabilization of aliphatic organic carbon by iron oxide. Sci Rep 5, 11214. https://doi.org/10.1038/srep11214

Agnelli, A., Corti, G., Massaccesi, L., Ventura, S., D'Acqui, L. P., 2021. Impact of biological crusts on soil formation in polar ecosystems. Geoderma, 401, 115340. https://doi.org/10.1016/j.geoderma.2021.115340

Baisden, W. T., Amundson, R., Cook, A. C., Brenner, D. L., 2002. Turnover and storage of C and N in five density fractions from California annual grassland surface soils. Global Biogeochemical Cycles, 16(4), 64-1.

Ballantyne, C. K. (1998). Age and significance of mountain-top detritus. *Permafrost and Periglacial Processes*, *9*(4), 327-345.

Berg, B., Meentemeyer, V., 2002. Litter quality in a north European transect versus carbon storage potential. Plant and Soil, 242(1), 83-92. https://doi.org/10.1023/A:1019637807021

Birks, H. J. B., & Willis, K. J. (2008). Alpines, trees, and refugia in Europe. *Plant Ecology & Diversity*, *1*(2), 147-160. https://doi.org/10.1080/17550870802349146

Birks, H.H., 1994. Plant macrofossils and the nunatak theory of per-glacial survival. *Dissertationes botanicae*, 234, 129–143.

Bockheim, J. G. (2007). Importance of cryoturbation in redistributing organic carbon in permafrost-affected soils. *Soil Science Society of America Journal*, *71*(4), 1335-1342. https://doi.org/10.2136/sssaj2006.0414N

Budge, K., Leifeld, J., Hiltbrunner, E., Fuhrer, J., 2011. Alpine grassland soils contain large proportion of labile carbon but indicate long turnover times. Biogeosciences, 8(7), 1911-1923. https://doi.org/10.5194/bg-8-1911-2011

Carcaillet, C., Blarquez, O. (2017). Fire ecology of a tree glacial refugium on a nunatak with a view on Alpine glaciers. *New Phytologist*, *216*, 1281–1290. https://doi.org/10.1111/nph.14721

Celi, L., Rosso, F., Freppaz, M., Agnelli, A., Zanini, E., 2010. Soil organic matter characteristics in sporadic permafrost-affected environment (Creux du Van, Switzerland). Arctic, Antarctic, and Alpine Research, 42(1), 1-8. https://doi.org/10.1657/1938-4246-42.1.1

Celi, L., Schnitzer, M., Nègre, M., 1997. Analysis of carboxyl groups in soil humic acids by a wet chemical method, Fourier-transform infrared spectrophotometry, and solution-state carbon-13 nuclear magnetic resonance. A comparative study. Soil Science, 162(3), 189-197.

Cerli, C., Celi, L., Kaiser, K., Guggenberger, G., Johansson, M.-B., Cignetti, A., Zanini, E., 2008. Changes in humic substances along an age sequence of Norway spruce stands planted on former agricultural land. Organic Geochemistry 39, 1269–1280. https://doi.org/10.1016/j.orggeochem.2008.06.001

Cerli, C., Celi, L., Kalbitz, K., Guggenberger, G., Kaiser, K., 2012. Separation of light and heavy organic matter fractions in soil—Testing for proper density cut-off and dispersion level. Geoderma, 170, 403-416. https://doi.org/10.1016/j.geoderma.2011.10.009

Conen, F., Zimmermann, M., Leifeld, J., Seth, B., Alewell, C. (2008). Relative stability of soil carbon revealed by shifts in δ 15 N and C: N ratio. *Biogeosciences*, *5*(1), 123-128.

D'Amico, M. E., Pintaldi, E., Catoni, M., Freppaz, M., & Bonifacio, E. (2019). Pleistocene periglacial imprinting on polygenetic soils and paleosols in the SW Italian Alps. *Catena*, *174*, 269-284.

D'Amico, M. E., Pintaldi, E., Sapino, E., Colombo, N., Quaglino, E., Stanchi, S., ... & Freppaz, M. (2020). Soil types of Aosta Valley (NW-Italy). *Journal of Maps*, *16*(2), 755-765. https://doi-org.bibliopass.unito.it/10.1080/17445647.2020.1821803

Dahl, E. (1987). The nunatak theory reconsidered. *Ecological bulletins*, 77-94. https://www.jstor.org/stable/20112974

Dai, X. Y., Ping, C. L., Candler, R., Haumaier, L., & Zech, W. 2001. Characterization of soil organic matter fractions of tundra soils in arctic Alaska by carbon-13 nuclear magnetic resonance spectroscopy. Soil Science Society of America Journal, 65(1), 87-93. https://doi.org/10.2136/sssaj2001.65187x

508 Dymov, A. A., Zhangurov, E. V., Hagedorn, F., 2015. Soil organic matter composition along altitudinal
509 gradients in permafrost affected soils of the Subpolar Ural Mountains. Catena, 131, 140-148.
510 https://doi.org/10.1016/j.catena.2015.03.020
511 European Commission, 1992. Council Directive 92/43/EEC of 21 May 1992 on the conservation of
512 natural habitats and of wild fauna and flora. Official Journal of the European Union 206, 7–50.
513 http://data.europa.eu/eli/dir/1992/43/oj
514 Nelson, P. N., Baldock, J. A., 2005. Estimating the molecular composition of a diverse range of natural
515 organic materials from solid-state ^{13}C NMR and elemental analyses. *Biogeochemistry*, *72(1)*,
516 1-34. https://doi-org.bibliopass.unito.it/10.1007/s10533-004-0076-3
517 Egli, M., Sartori, G., Mirabella, A., et al. (2009). Effect of north and south exposure on organic matter
518 in high Alpine soils. *Geoderma* *149*(1-2), 124–136.
519 https://doi.org/10.1016/j.geoderma.2008.11.027
520 Eusterhues, K., Rumpel, C., Kleber, M., Kögel-Knabner, I., 2003. Stabilisation of soil organic matter
521 by interactions with minerals as revealed by mineral dissolution and oxidative degradation.
522 Organic Geochemistry, 34(12), 1591-1600. https://doi.org/10.1016/j.orggeochem.2003.08.007
523 Fairbridge R.W. (1968). Glacial refuges (nunatak theory). In: *Geomorphology*. *Encyclopedia of Earth*
524 *Science*. Springer, Berlin, Heidelberg.
525 Favilli, F., Egli, M., Brandova, D., et al. (2009). Combined use of relative and absolute dating
526 techniques for detecting signals of Alpine landscape evolution during the late Pleistocene and
527 early Holocene. *Geomorphology*, 112, 48–66.
528 https://doi.org/10.1016/j.geomorph.2009.05.003
529 Favilli, F., Egli, M., Cherubini, P., et al. (2008). Comparison of different methods of obtaining a
530 resilient organic matter fraction in Alpine soils. *Geoderma*, 145, 355–369.
531 https://doi.org/10.1016/j.geoderma.2008.04.002

Freppaz, M., Celi, L., Marchelli, M., Zanini, E., 2008. Snow removal and its influence on temperature and N dynamics in alpine soils (Vallee d'Aoste, northwest Italy). Journal of Plant Nutrition and Soil Science, 171(5), 672-680.

Freppaz, M., Williams, M.W., Gabrieli, J. et al., 2021. Characterization of organic-rich mineral debris revealed by rapid glacier retreat, Indren Glacier, European Alps. J. Mt. Sci. 18, 1521–1536. https://doi.org/10.1007/s11629-020-6288-8

Golchin, A., Oades, J. M., Skjemstad, J. O., Clarke, P., 1994. Study of free and occluded particulate organic matter in soils by solid state 13C CP/MAS NMR spectroscopy and scanning electron microscopy. Soil Research, 32(2), 285-309. https://doi.org/10.1071/SR9940285

Goodfellow, B. W. (2007). Relict non-glacial surfaces in formerly glaciated landscapes. *Earth-Science Reviews*, 80(1-2), 47-73. https://doi.org/10.1016/j.earscirev.2006.08.002

Gubin S., Lupachev A.V. (2008). Soil formation and the underlying permafrost. *Eurasian Soil Science 41*(6):655-667.

Hall, S. J., Silver, W. L., Timokhin, V. I., and Hammel, K. E. (2016). Iron addition to soil specifically stabilized lignin, *Soil and Biology Biochemistry*, *98*, 95–98, https://doi.org/10.1016/j.soilbio.2016.04.010.

Hättestrand, C., & Stroeven, A. P. (2002). A relict landscape in the centre of Fennoscandian glaciation: Geomorphological evidence of minimal Quaternary glacial erosion. *Geomorphology*, *44*(1-2), 127-143. https://doi.org/10.1016/S0169-555X(01)00149-0

Helfrich, M., Flessa, H., Mikutta, R., Dreves, A., Ludwig, B., 2007. Comparison of chemical fractionations methods for isolating stable soil organic carbon pools. European Journal of Soil Science. https://doi.org/10.1111/j.1365-2389.2007.00926.x.

Hobbie, S. E., Schimel, J. P., Trumbore, S. E., and Randerson, J. R., 2000. Controls over carbon storage and turnover in highlatitude soils. Global Change Biology, 6: 196–210. https://doi.org/10.1046/j.1365-2486.2000.06021.x

557 IUSS Working Group WRB, 2015. World Reference Base for Soil Resources 2014, update 2015.
558 International soil classification system for naming soils and creating legends for soil maps.
559 *World Soil Resources, Reports No. 106*, FAO, Rome. E-ISBN 978-92-5-108370-3
560 Kaiser, K., Mikutta, R., & Guggenberger, G. (2007). Increased stability of organic matter sorbed to
561 ferrihydrite and goethite on aging. *Soil Science Society of America Journal*, *71*(3), 711-719.
562 https://doi.org/10.2136/sssaj2006.0189
563 Kauffman, J. B. and Pyke, D. A. (2001). Range ecology, global livestock influences. *Encyclopedia of*
564 *Biodiversity* ed S Levin (San Diego, CA: Academic) vol 5 pp 33–52.
565 Kelleher, B. P., Simpson, A. J., 2006. Humic substances in soils: are they really chemically distinct?
566 *Environmental science & technology*, 40(15), 4605-4611. https://doi.org/10.1021/es0608085
567 Kleber, M., Bourg, I. C., Coward, E. K., Hansel, C. M., Myneni,S. C. B., Nunan, N. (2021). Dynamic
568 interactions at the mineral– organic matter interface, Nat. Rev. Earth Environ., 2, 402–421,
569 https://doi.org/10.1038/s43017-021-00162-y, 2021.
570 Kosiński, P., Sękiewicz, K., Walas, Ł., Boratyński, A., & Dering, M. (2019). Spatial genetic structure
571 of the endemic alpine plant Salix serpillifolia: genetic swamping on nunataks due to
572 secondary colonization?. *Alpine Botany*, 129(2), 107-121. https://doi-
573 org.bibliopass.unito.it/10.1007/s00035-019-00224-4
574 Kramer, M. G., Sanderman, J., Chadwick, O. A., Chorover, J., and Vitousek, P. M. (2012). Long-term
575 carbon storage through retention of dissolved aromatic acids by reactive particles in soil, *Global*
576 *Change Biology*, *18*, 2594–2605, https://doi.org/10.1111/j.1365- 2486.2012.02681.x.
577 Li, C., Cao, Z., Chang, J., Zhang, Y., Zhu, G., Zong, N., He, Y., Zhang, J., He, N., 2017. Elevational
578 gradient affect functional fractions of soil organic carbon and aggregate stability in a Tibetan
579 alpine meadow. Catena, 156, 139-148. https://doi.org/10.1016/j.catena.2017.04.007
580 Lodygin, E.D., Beznosikov, V.A. & Vasilevich, R.S. (2014). Molecular composition of humic
581 substances in tundra soils (^{13}C-NMR spectroscopic study). *Eurasian Soil Science*, *47*, 400–406.
582 https://doi.org/10.1134/S1064229314010074

583 Lupachev A., Abakumov E., Gubin S. (2017). The influence of cryogenic mass exchange on the
584 composition and stabilization rate of soil organic matter in Cryosols of the Kolyma Lowland
585 (North Yakutia, Russia). *Geosciences*, 7, 24.
586 Mainetti, A., D'Amico, M., Probo, M., Quaglia, E., Ravetto Enri, S., Celi, L., Lonati, M. (2021).
587 Successional Herbaceous Species Affect Soil Processes in a High-Elevation Alpine Proglacial
588 Chronosequence. *Frontiers in Environmental Science*, 284.
589 https://doi.org/10.3389/fenvs.2020.615499
590 Mainka, M., Summerauer, L., Wasner, D., Garland, G., Griepentrog, M., Berhe, A. A., Doetterl, S.
591 (2021). Soil geochemistry as a driver of soil organic matter composition: insights from a soil
592 chronosequence. *Biogeosciences Discussions*, 1-23.
593 Marin-Spiotta, E., Chaopricha, N. T., Mueller, C., Diefendorf, A. F., Plante, A. F., Grandy, S., Mason,
594 J. A., 2012. Stabilization of ancient organic matter in deep buried paleosols. In AGU Fall
595 Meeting Abstracts (Vol. 2012, pp. B13A-0484). 2012AGUFM.B13A0484M
596 McCarroll, D., Ballantyne, C.K., Nesje, A., Dahl, S.O. (1995). Nunataks of the last ice sheet in
597 northwest Scotland. *Boreas*, 24, 305–323. https://doi.org/10.1111/j.1502-
598 3885.1995.tb00782.x
599 Meentemeyer, V., Box, E. O., and Thompson, R., 1982. World patterns and amounts of terrestrial plant
600 litter production, Bioscience, 32, 125–128. https://doi.org/10.2307/1308565
601 Mehra, O. P. and Jackson, M. L. (1960). Fe oxide removal from soils and clays by a dithionite-citrate
602 system buffered with sodium bicarbonate: in Proc. 7th Natl. Conf. on Clays and Clay Minerals,
603 Swineford, A., ed., Pergamon Press, Washington, DC, 317-327.
604 Mercalli, L. (2004). Il clima terrestre negli ultimi 10'000 anni. https://doi.org/10.5169/seals-132929
605 Merino, A., Fonturbel, M. T., Fernández, C., Chávez-Vergara, B., García-Oliva, F., Vega, J. A. (2018).
606 Inferring changes in soil organic matter in post-wildfire soil burn severity levels in a temperate
607 climate. *Science of the Total Environment, 627*, 622-632.

608 Mikutta, R., Kleber, M., Torn, M.S. et al., 2006. Stabilization of Soil Organic Matter: Association with
609 Minerals or Chemical Recalcitrance? Biogeochemistry 77**,** 25–56.
610 https://doi.org/10.1007/s10533-005-0712-6
611 Monson, J., Chua, T., Thompson, M.L., Betttis, E.A., 2011. Characterization of SOM in Holocene
612 paleosols, Minnesota, 9–12 October, 2011. Annual Meeting in Minneapolis. Geological Society
613 of America (GSA) (Paper No. 258-1.). https://doi.org/10.1016/j.geoderma.2014.01.028
614 Nelson, P. N., Baldock, J. A., 2005. Estimating the molecular composition of a diverse range of natural
615 organic materials from solid-state ^{13}C NMR and elemental analyses. Biogeochemistry, 72(1),
616 1-34. https://doi.org/10.1007/s10533-004-0076-3
617 Oddi, L., Celi, L., Cremonese, E., Filippa, G., Galvagno, M., Palestini, G., Siniscalco, C., 2019.
618 Decomposition processes interacting with microtopography maintain ecosystem heterogeneity
619 in a subalpine grassland. Plant and Soil, 434(1), 379-395. https://doi.org/10.1007/s11104-018-
620 3842-z
621 Orombelli, G. (2011). Holocene mountain glacier fluctuations: a global overview. *Geografia Fisica e*
622 *Dinamica Quaternaria 34*(1), 17–24.
623 Paus, A., Velle, G., Larsen, J., et al., 2006. Lateglacial nunataks in central Scandinavia:
624 Biostratigraphical evidence for ice thickness from Lake Flåfattjønn, Tynset, Norway.
625 *Quaternary Science. Reviews, 25*, 1228–1246.
626 https://doi.org/10.1016/j.quascirev.2005.10.008
627 Piccolo, A., Stevenson, F. J. (1982). Infrared spectra of Cu2+ Pb2+ and Ca2+ complexes of soil humic
628 substances. Geoderma, 27(3), 195-208. https://doi.org/10.1016/0016-7061(82)90030-1
629 Pintaldi E., D'Amico Michele E., Colombo N, Colombero C., Sambuelli L., De Regibus C., Franco D.,
630 Perotti L., Freppaz M., 2021a. Hidden soils and their carbon stocks at high-elevation
631 ecosystems in the European Alps (NW-Italy). CATENA, 198.
632 https://doi.org/10.1016/j.catena.2020.105044

633 Pintaldi, E., D'Amico, M. E., Colombo, N., Martinetto, E., Said-Pullicino, D., Giardino, M., Freppaz,
634 M., 2021b. Hidden paleosols on a high-elevation Alpine plateau (NW Italy): Evidence for
635 Lateglacial Nunatak? Global and Planetary Change, 207, 103676.
636 https://doi.org/10.1016/j.gloplacha.2021.103676
637 Saggar, S., Parshotam, A., Sparling, G. P., Feltham, C. W., Hart, P. B. S., 1996. 14C-labelled ryegrass
638 turnover and residence times in soils varying in clay content and mineralogy. Soil Biology and
639 Biochemistry, 28(12), 1677-1686.
640 Schnitzer, M., 1982. Organic matter characterization. In Page, A. L. et al. (eds.), Methods of Soil
641 Analysis Part 2. Second Edition. Agronomy 9. Madison, Wisconsin: American Society of
642 Agronomy and Soil Science Society of America.
643 Schönswetter, P., Stehlik, I., Holderegger, R., et al., 2005. Molecular evidence for glacial refugia of
644 mountain plants in the European Alps. *Molecular Ecology. 14*, 3547–3555.
645 https://doi.org/10.1111/j.1365-294X.2005.02683.x
646 Schwertmann, U. (1964) Differenzierung der Eisenoxide des Bodens durch Extraktion mit einer
647 Ammonium Oxalat LS- sung: Z. *Pflanzenerniihr. Diing. Bodenkd*. 105, 194-202.
648 Shiau, YJ., Chen, JS., Chung, TL. et al. (2017). 13C NMR spectroscopy characterization of particle-
649 size fractionated soil organic carbon in subalpine forest and grassland ecosystems. *Botanical*
650 *Studies, 58,* 23. https://doi-org.bibliopass.unito.it/10.1186/s40529-017-0179-5
651 Sodano, M., Said-Pullicino, D., Fiori, A.F., Martin, M., Celi, L., 2016. Sorption of paddy soil-derived
652 dissolved organic matter on hydrous iron oxide-vermiculite mineral phases Geoderma, 2016,
653 261, pp. 169–177. https://doi.org/10.1016/j.geoderma.2015.07.014
654 Stützer, A., 1999. Podzolization as a soil forming process in the alpine belt of Rondane, Norway.
655 Geoderma 91, 237–248. https://doi.org/10.1016/S0016-7061(99)00009-9
656 Tan, Z., Lal, R., Owens, L., Izaurralde, R. C. (2007). Distribution of light and heavy fractions of soil
657 organic carbon as related to land use and tillage practice. Soil and Tillage Research, 92(1-2),
658 53-59. https://doi.org/10.1016/j.still.2006.01.003

659 Tognetto, F., Perotti, L., Viani, C., et al. (2021). Geomorphology and geosystem services of the Indren-
660 Cimalegna area (Monte Rosa massif – Western Italian Alps). *Journal of Maps 17*(2), 161–172.
661 DOI:10.1080/17445647.2021.1898484
662 Hormes, A., Karlén, W., & Possnert, G. (2004). Radiocarbon dating of palaeosol components in
663 moraines in Lapland, northern Sweden. *Quaternary Science Reviews*, *23*(18-19), 2031-2043.
664 https://doi.org/10.1016/j.quascirev.2004.02.004
665 Van Vliet-Lanoé, B. (1998). Pattern ground, hummocks, and Holocene climate changes. *Eurasian soil*
666 *science*, *31*(5), 507-513.
667 Wagai, R.,Mayer, L.M., Kitayama, K., 2009. Nature of the "occluded" low-density fraction in soil
668 organic matter studies: a critical review. *Soil Science and Plant Nutrition 55*, 13–25. https://doi-
669 org.bibliopass.unito.it/10.1111/j.1747-0765.2008.00356.x
670 Weintraub, M. N., and Schimel, J. P., 2003. Interactions between carbon and nitrogen mineralization
671 and soil organic matter chemistry in arctic tundra soils. *Ecosystems*, *6*: 87–93.
672 https://doi.org/10.1007/s10021-002-0124-6
673 White, D. M., Garland, D. S., Ping, C. L., & Michaelson, G., (2004). Characterizing soil organic matter
674 quality in arctic soil by cover type and depth. Cold Regions Science and Technology, 38(1),
675 63-73. https://doi.org/10.1016/j.coldregions.2003.08.001
676 Wiseman, C. L. S., Püttmann, W. (2006). Interactions between mineral phases in the preservation of
677 soil organic matter. *Geoderma*, *134*(1-2), 109-118.
678 https://doi.org/10.1016/j.geoderma.2005.09.001
679 Xu, C., Guo, L., Ping, C. L., White, D. M., (2009). Chemical and isotopic characterization of size-
680 fractionated organic matter from cryoturbated tundra soils, northern Alaska. *Journal of*
681 *Geophysical Research: Biogeosciences*, *114*(G3). https://doi.org/10.1029/2008JG000846
682 Zhou, Z., Chen, N., Cao, X., Chua, T., Mao, J., Mandel, R. D., ... & Thompson, M. L. (2014).
683 Composition of clay-fraction organic matter in Holocene paleosols revealed by advanced solid-

state NMR spectroscopy. *Geoderma, 223*, 54-61. https://doi.org/10.1016/j.geoderma.2014.01.028

Ziegler, F., Zech, W. (1989). Distribution pattern of total lipids and lipid fractions in forest humus. *Zeitschrift für Pflanzenernährung und Bodenkunde, 152*(3), 287-290. https://doi.org/10.1002/jpln.19891520304

Figures

Figure 1

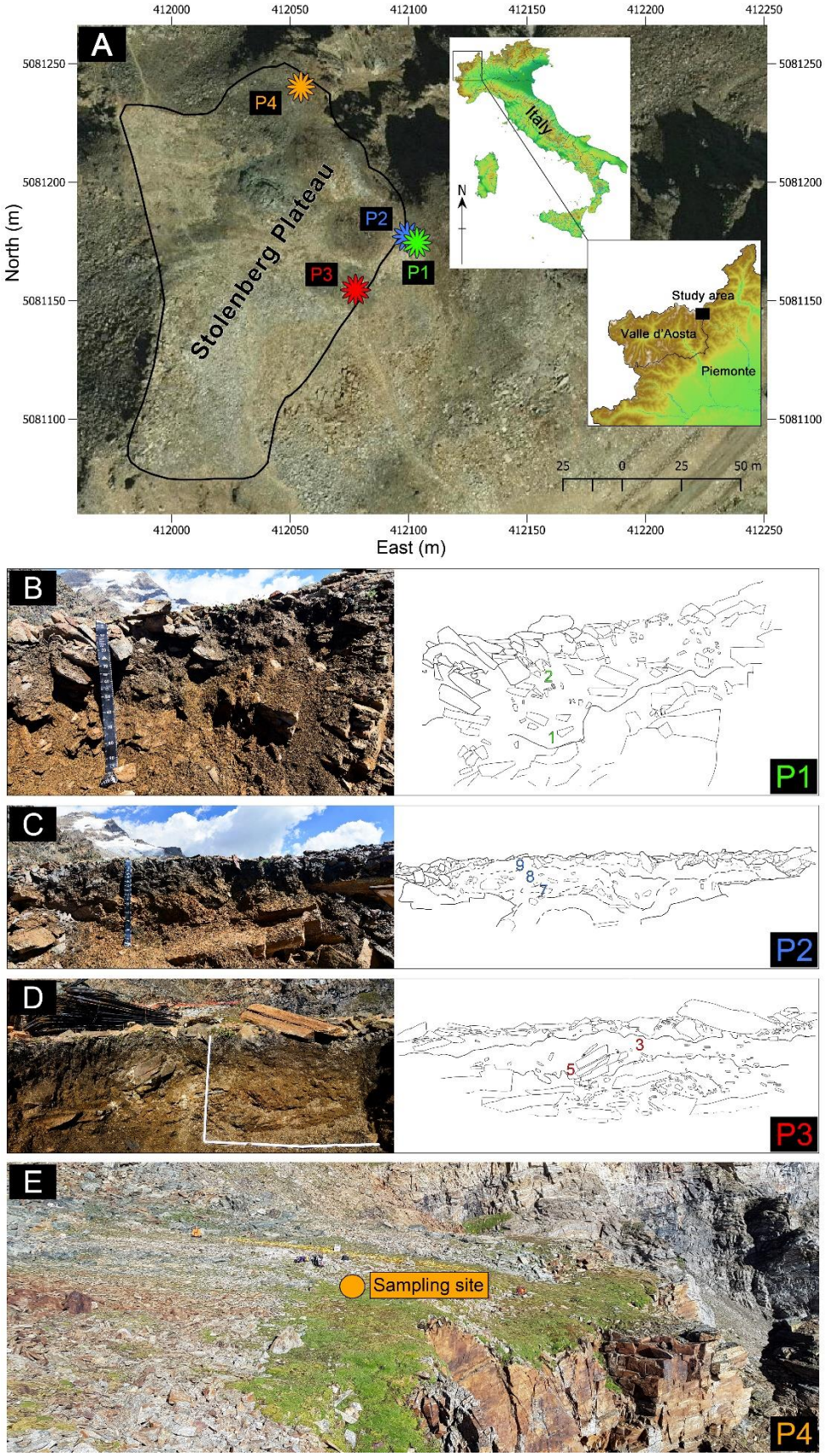

Figure 2

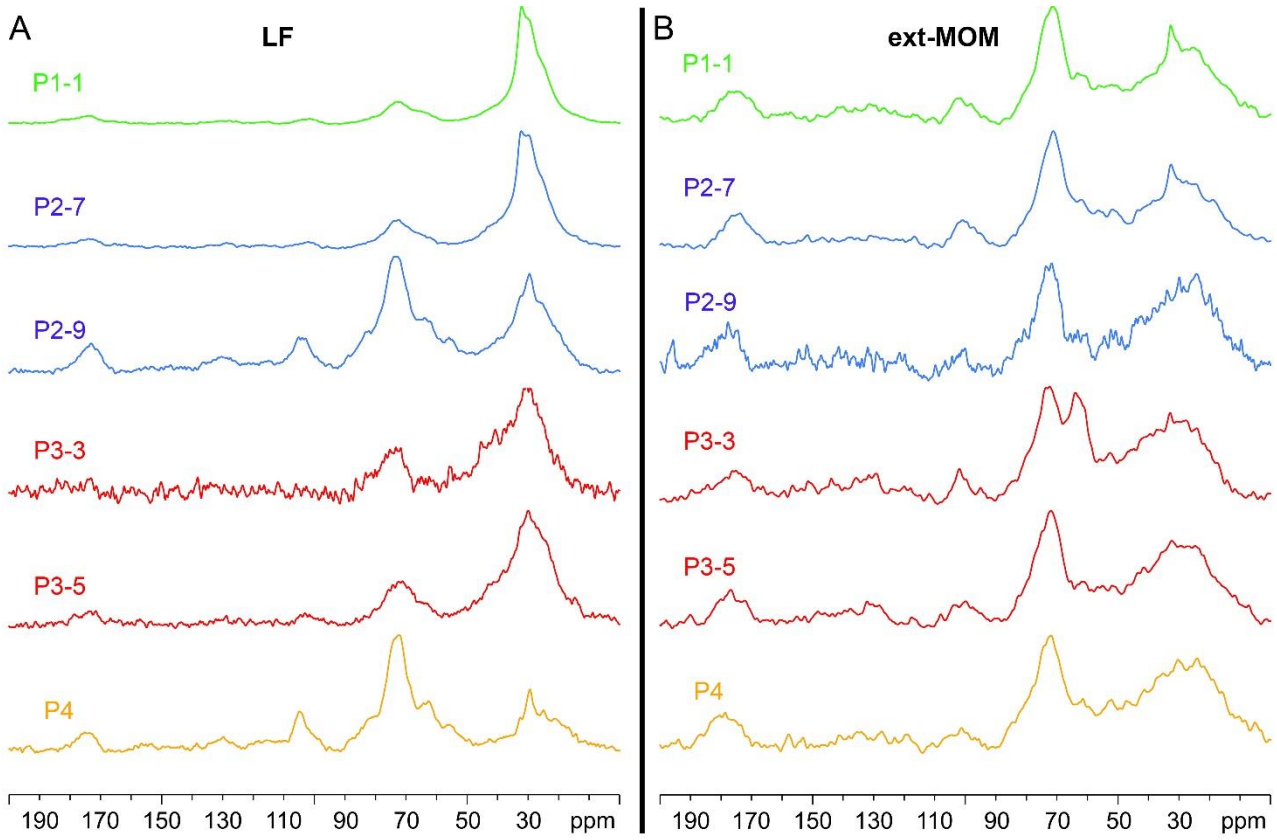

Figure 3

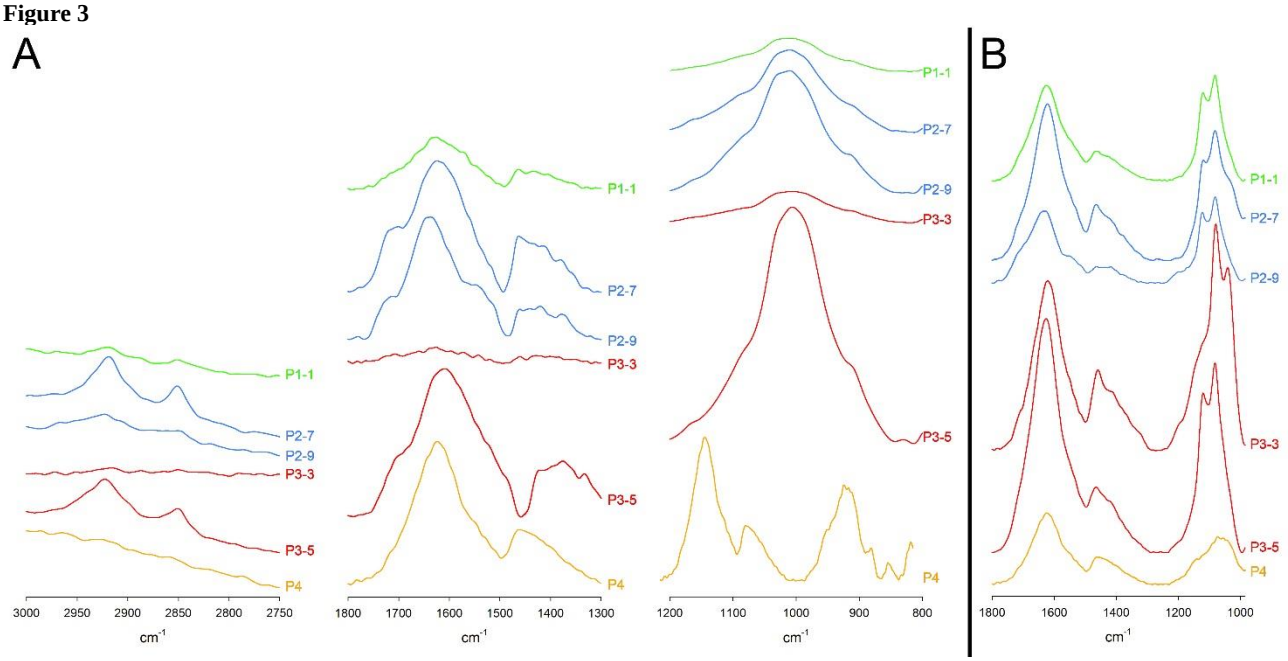

Figures captions

Figure 1. (A) Location of the study area in the NW Italian Alps (www.pcn.minambiente.it) and overview of the study area (orthoimage Piemonte Region, year 2010) (coordinate system WGS 84 / UTM zone 32N); the forms indicate the location of the three soil profiles (P1, P2, and P3) and the vegetated patch (P4); (B, C, and D) soil profiles, with the corresponding scheme (right) reporting sampling points (number) and the horizon limits (lines therein); (E) sampling site in the vegetated patch.

Figure 2. NMR spectra of (A) LF and (B) ext-MOM fractions.

Figure 3. (A) FT-IR spectra of LF samples (range 3000-2750, 1800-1300, and 1200-800); (B) ext-MOM fractions (range 1800-1000).

Tables

Table 1. Main physical and chemical properties of the soil samples. LS=loamy sand; SL=sandy loam. *Data from Pintaldi et al. (2021a).

Sample number	Horizon*	Textural class*	pH*	Fe_o (g kg^{-1})	Al_o (g kg^{-1})	Fe_d (g kg^{-1})	0.5* Fe_o +Al_o	Fe_o/Fe_d	pH NaF
1-1	**A2**	LS	4.8	2.54	2.98	22.94	0.31	0.11	9.7
1-2	**A1**	LS	4.4	2.44	1.30	21.77	0.14	0.11	8.5
2-7	**A@**	LS	5.6	2.58	2.36	18.23	0.25	0.14	10.0
2-8	**A2**	LS	4.7	1.35	1.87	18.72	0.19	0.07	9.5
2-9	**A1**	LS	4.4	2.15	1.13	18.70	0.12	0.12	8.3
3-3	**A2**	LS	4.9	2.90	1.54	14.70	0.17	0.20	8.8
3-5	**A2**	SL	4.7	2.70	2.03	14.46	0.22	0.19	10.0
P4	**A**	LS	4.5	4.48	1.33	12.20	0.37	0.37	8.7

Table 2. Density and chemical fractionation results: Total Organic Carbon (TOC) and Total Nitrogen (TN) in bulk soil samples; Carbon (C), Nitrogen (N), C/N ratio, and relative C distribution % in the different fraction. LF: Light Fraction; MOM: Mineral Organic Matter.[1]Calculated as percent of C of MOM fraction; [2]Calibrated radiocarbon ^{14}C ages of bulk soil sample from Pintaldi et al. (2021b).

Sample	Cover type	Bulk soil			LF			MOM			Ext-MOM			C distribution %			N distribution %			Age cal. ka BP[2]
		TOC g/kg	TN g/kg	TOC /TN	C g/kg	N g/kg	C/N	C g/kg	N g/kg	C/N	C g/kg	N g/kg	C/N	LF	MOM	ext-MOM[1]	LF	MOM	ext-MOM[1]	
P1-1	Blockfield/Blockstream	20.5	1.4	15	220.0	7.6	29	11.9	0.8	15	572.6	49.2	12	12.8	87.2	47.3	7.0	93.0	60.4	8.6
P1-2	Blockfield/Blockstream	12.2	1.2	10	180.0	8.4	21	9.3	0.8	12	482.2	57.3	8	6.1	93.9	43.3	3.4	96.6	59.8	5.7
P2-7	Blockfield/Blockstream	19.3	1.4	13	236.1	7.9	30	15.0	1.1	13	601.0	50.3	12	7.4	92.6	41.5	3.5	96.5	47.4	6.4
P2-8	Blockfield/Blockstream	12.3	1.1	11	205.4	7.0	30	9.9	0.9	11	451.7	44.8	10	4.5	95.5	37.7	1.7	98.3	41.1	8.4
P2-9	Blockfield/Blockstream	12.5	1.4	9	217.2	14.3	15	8.5	1.0	9	464.8	57.7	8	14.3	85.7	23.7	8.5	91.5	25.0	17.7
P3-3	Blockfield/Blockstream	10.6	1.0	10	122.5	5.0	24	7.2	0.7	10	487.1	49.5	10	3.1	96.9	45.6	1.3	98.7	47.7	21.8
P3-5	Blockfield/Blockstream	13.1	1.3	10	127.5	5.4	24	9.4	0.8	11	597.0	60.6	10	5.4	94.6	42.4	2.7	97.3	50.6	13.2
P4	Vegetated patch	13.8	2.3	6	311.6	13.9	22	8.6	1.0	9	577.6	79.1	7	9.1	90.9	46.4	3.7	96.3	54.6	4.2

Table 3. Integration areas for the major C-types in the ^{13}C NMR spectra of LF samples.

LF	- COOH 166-190	Phenolic-OH 156–165	Aromatic C 111–155	Saccharidic C 61–110	O-C, N-C 46-60	-CH_2- 0-45	$\frac{Alkyl\ C}{O\ Alkyl\ C}$
P1-1	4.1	0.1	0.4	16.5	3.5	75.4	4.6
P2-7	3.7	0.4	0.6	16.5	3.5	75.3	4.6
P2-9	5.2	0.2	7.2	44.8	8.6	34.0	0.8
P3-3	5.7	1.1	6.7	15.2	6.9	64.4	4.2
P3-5	4.7	1.0	3.0	21.3	6.2	63.8	3.0
P4	5.1	0.7	8.7	52.5	7.9	25.1	0.5

Table 4. Integration areas for the major C-types in the ^{13}C NMR spectra of ext-MOM.

Ext-MOM	- COOH 166-190	Phenolic-OH 156–165	Aromatic C 111–155	Saccharidic C 61–110	O-C, N-C 46-60	-CH_2- 0-45	$\frac{Alkyl\ C}{O\ Alkyl\ C}$
P1-1	7.5	0.5	3.2	34.3	10.9	43.6	1.3
P2-7	8.4	0.8	5.9	36.7	10.5	37.7	1.0
P2-9	9.1	0.3	4.2	28.5	7.9	50.0	1.8
P3-3	5.0	0.3	6.8	37.1	13.6	37.2	1.0
P3-5	4.2	0.0	2.5	35.5	11.9	45.9	1.3
P4	7.9	0.2	3.5	31.6	11.0	45.8	1.4